ACCOUNTS of chemical research

pubs.acs.org/accounts Article

Toward Accurate Photoluminescence Nanothermometry Using Rare-Earth Doped Nanoparticles for Biomedical Applications

Miao Liu, Jinyang Liang,* and Fiorenzo Vetrone*

Cite This: *Acc. Chem. Res.* 2024, 57, 2653−2664 Read Online

ACCESS | Metrics & More | Article Recommendations

CONSPECTUS: Photoluminescence nanothermometry can detect the local temperature at the submicrometer scale with minimal contact with the object under investigation. Owing to its high spatial resolution, this technique shows great potential in biomedicine in both fundamental studies as well as preclinical research. Photoluminescence nanothermometry exploits the temperature-dependent optical properties of various nanoscale optical probes including organic fluorophores, quantum dots, and carbon nanostructures. At the vanguard of these diverse optical probes, rare-earth doped nanoparticles (RENPs) have demonstrated remarkable capabilities in photoluminescence nanothermometry. They distinguish themselves from other luminescent nanoprobes owning to their unparalleled and versatile optical properties that include narrow emission bandwidths, high photostability, tunable lifetimes from microseconds to milliseconds, multicolor emissions spanning the ultraviolet, visible, and near-infrared (NIR) regions, and the ability to undergo upconversion, all with excitation of a single, biologically friendly NIR wavelength. Recent advancements in the design of novel RENPs have led to new fundamental breakthroughs in photoluminescence nanothermometry. Moreover, driven by their excellent biocompatibility, both *in vitro* and *in vivo*, their implementation in biomedical applications has also gained significant traction. However, these nanoprobes face limitations caused by the complex biological environments, including absorption and scattering of various biomolecules as well as interference from different tissues, which limit the spatial resolution and detection sensitivity in RENP temperature sensing.

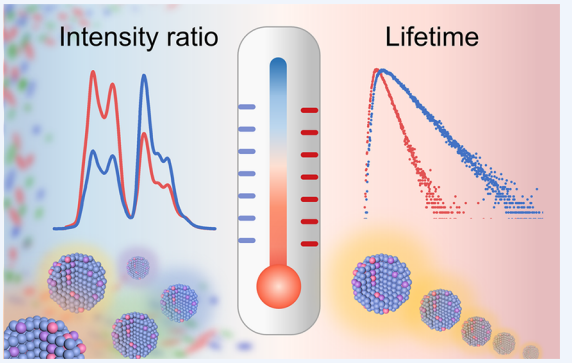

Among existing approaches in RENP photoluminescence nanothermometry, the most prevalent implemented mechanisms either leverage the changes in the relative intensity ratio of two emission bands or exploit the lifetimes of various excited states. Photoluminescence intensity ratio (PLIR) nanothermometry has been the mainstream method owing to the readily available spectrometers for photoluminescence acquisition. Despite offering high temperature sensitivity and spatial resolution, this technique is restricted by tedious calibration and undesirable fluctuation in photoluminescence intensity ascribed to factors such as probe concentration, excitation power density, and biochemical surroundings. Lifetime-based nanothermometry uses the lifetime of a specific transition as the contrast mechanism to infer the temperature. This modality is less susceptible to various experimental factors and is compatible with a broader range of photoluminescence nanoprobes. However, due to relatively expensive and complex instrumentation, long data acquisition, and sophisticated data analysis, lifetime-based nanothermometry is still breaking ground with recently emerging techniques lightening its path.

In this *Account*, we provide an overview of RENP nanothermometry and their applications in biomedicine. The architectures and luminescence mechanisms of RENPs are examined, followed by the principles of PLIR and lifetime-based nanothermometry. The in-depth description of each approach starts with its basic principle of accurate temperature sensing, followed by a critical discussion of the representative techniques, applications as well as their strengths and limitations. Special emphasis is given to the emerging modality of lifetime-based nanothermometry in light of the important new developments in the field. Finally, a summary and an outlook are provided to conclude this *Account*.

KEY REFERENCES

- Hazra, C.; Skripka, A.; Ribeiro, S. J. L.; Vetrone, F. Erbium Single-Band Nanothermometry in the Third Biological Imaging Window: Potential and Limitations. *Adv. Optical Mater.* **2020**, *8* (23), 2001178−2001186.[1] A

Received: June 5, 2024
Revised: August 16, 2024
Accepted: August 16, 2024
Published: August 28, 2024

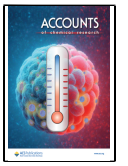

https://doi.org/10.1021/acs.accounts.4c00342
Acc. Chem. Res. 2024, 57, 2653−2664

single-center PLIR nanothermometer using Stark sublevels of Er^{3+} in the NIR-IIb region.

- Skripka, A.; Karabanovas, V.; Jarockyte, G.; Marin, R.; Tam, V.; Cerruti, M.; Rotomskis, R.; Vetrone, F. Decoupling Theranostics with Rare Earth Doped Nanoparticles. *Adv. Funct. Mater.* **2018**, *29* (12), 1807105−1807116.[2] A multilayered core−shell RENP, which could be orthogonally triggered under 980 and 808 nm for on-demand therapy and diagnostics.
- Liu, X.; Skripka, A.; Lai, Y.; Jiang, C.; Liu, J.; Vetrone, F.; Liang, J. Fast Wide-field Upconversion Luminescence Lifetime Thermometry Enabled by Single-shot Compressed Ultrahigh-speed Imaging. *Nat. Commun.* **2021**, *12* (1), 6401−6409.[3] Video-rate temperature sensing in the wide field moving biological sample via single-shot using upconversion photoluminescence lifetime-based nanothermometry.
- Skripka, A.; Morinvil, A.; Matulionyte, M.; Cheng, T.; Vetrone, F. Advancing Neodymium Single-band Nanothermometry. *Nanoscale* **2019**, *11* (23), 11322−11330.[4] Three emission bands of Nd^{3+} in NIR-I and NIR-IIa range were investigated as PLIR nanothermometry and each emission was evaluated for reliable temperature readout.
- Liu, M.; Lai, Y.; Marquez, M.; Vetrone, F.; Liang, J. Short-Wave Infrared Photoluminescence Lifetime Mapping of Rare-Earth Doped Nanoparticles Using All-Optical Streak Imaging. *Adv. Sci.*. **2023**, *11* (11), 2305284−2305292.[5] A NIR streak camera with tunable imaging speed to map the photoluminescence lifetime of RENPs and application in lifetime-based nanothermometry.

1. INTRODUCTION

Temperature is one of the most important biomarkers in biology. It directly affects innumerable processes in the body including metabolic rate, gene expression, immune reaction, cell cycle, and apoptosis.[6−8] Monitoring temperature could thus be a feasible and effective way to study basic biological functions (e.g., brain activity and enzyme activity) where the temperature variations are minute (ca. 1 °C).[7,9] Furthermore, the first sign of most illnesses (e.g., cancer, infection, inflammation, and cardiovascular conditions) is the presence of a thermal gradient,[10−12] and hence temperature sensing can potentially be of great value in disease detection. In this context, measuring temperature with high reliability and accuracy is in urgent demand. These requirements have driven the development of temperature measurement from the previous generation of contact, invasive, microscale level thermometers (e.g., thermocouple) to new remote control, minimally invasive, submicrometer scale thermometers (e.g., photoluminescent nanothermometers).[13]

Photoluminescent nanothermometers have been recognized as promising candidates for accurate and dynamic temperature measurement with specific emphasis on applications in biomedicine.[14,15] Photoluminescence nanothermometry is based on the optical performance of the probe, which will be influenced by its surrounding temperature, establishing a correlation between its photoluminescence properties and temperature. A variety of nanoscale optical probes have been studied for photoluminescence nanothermometry, for example, organic fluorophores, quantum dots, and diverse carbon nanostructures.[15−17] Among these studied photoluminescent probes, rare-earth doped complexes and nanoparticles have shown great promise for nanothermometry. In particular, RENPs are at the forefront as they have high photostability, low toxicity, and the relative ease of biofunctionalization such that their surfaces could be altered by specific biological moieties.[18,19] Most importantly, RENPs present unique optical properties, such as narrow 4*f*-4*f* transition bandwidths, long lifetimes, and high resistance to interference from the surrounding environment.[18−20] When excited with NIR wavelengths, RENPs possess multiple emissions in the ultraviolet to visible ranges (anti-Stokes photoluminescence). This multiphoton excitation process, whereby two or more NIR excitation photons are converted into a single higher energy photon, is known as upconversion and in a biomedical context, can be exploited to trigger other light-activated modalities. Additionally, following excitation with the same NIR wavelengths, RENPs can also emit light further in the NIR region (Stokes photoluminescence) that is often referred to as downshifting photoluminescence (different from downconversion, in which one higher energy photon is converted into two or more lower energy photons). In particular, their ability to be excited but also emit in the NIR region makes them especially suitable for deep tissue imaging and nanothermometry. These distinguishing properties showcase their versatility and allow RENPs to stand out from their counterparts.

Temperature-dependent optical changes of nanothermometers can be observed with both steady-state and time-resolved photoluminescence measurements. Normally, the working principle for photoluminescence nanothermometry includes changes in the probes' polarization anisotropy, photoluminescence intensity, peak position, bandwidth, bandshape, and lifetime.[13] Polarization anisotropy is often observed in very specific cases while nanothermometry using photoluminescence peak position has been reported with relative success in semiconductor quantum dots.[15,16] Photoluminescence intensity-based temperature sensing from a single peak is easy and simple but can be prone to measurement anomalies caused by intensity variations, which may lead to inaccurate temperature readouts.[21] In the case of RENPs, the photoluminescence peak position and bandwidth present only subtle differences at varying temperatures due to the shielding effect of the rare-earth ions.[13,16,20] Consequently, the photoluminescence bandshape where the PLIR between two peaks or two transitions has gradually become the established method in photoluminescence nanothermometry. Following astonishing growth in RENP nanothermometry, the PLIR technique has become the most widely studied method and presents high temperature and spatial resolution for various applications with a specific emphasis on biomedicine. In contrast, RENP lifetime-based nanothermometry, while still in its infancy because of the aforementioned issues, has been recognized as a potential technique for accurate temperature sensing with less biased error.[3,12] Taken together, there is a concerted effort to make lifetime-based nanothermometry more user-friendly, potentially moving it closer to translational applications.

In this Account, we provide an overview of PLIR and lifetime-based nanothermometry using RENPs and focus on their path toward accurate temperature sensing in biomedicine. The basic theory and working principles of each approach will be discussed and representative examples will be demonstrated. A critical discussion of the advantages as well as the presence

https://doi.org/10.1021/acs.accounts.4c00342
Acc. Chem. Res. 2024, 57, 2653−2664

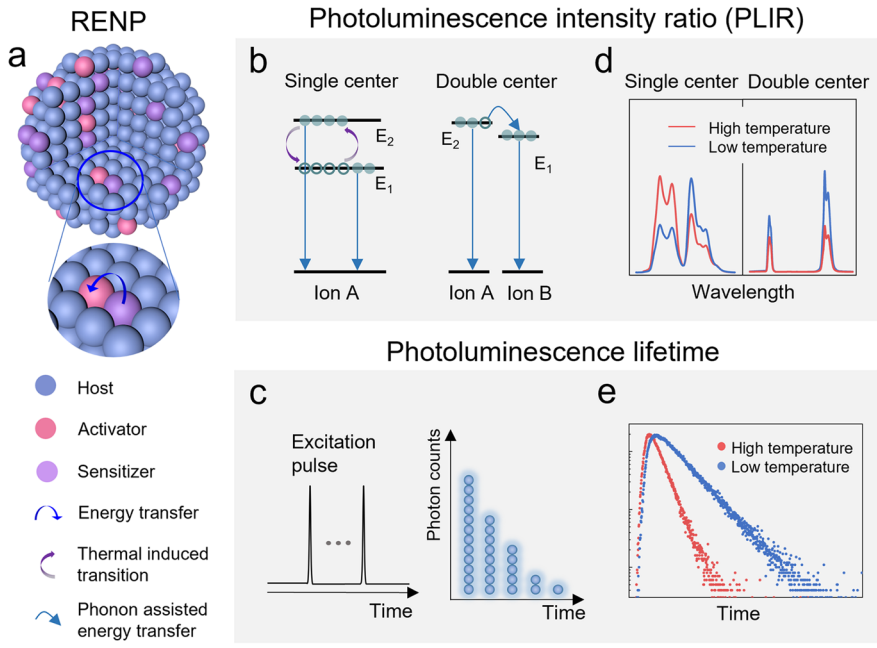

Figure 1. (a) Typical structure of RENPs. (b, c) Basic working principles of PLIR[13,15,16] (b) and lifetime-based (c) nanothermometry, respectively. (d, e) Schematic representations of the PLIR[16] (d) and lifetime curves (e) at different temperatures, respectively.

of possible limitations during the temperature detection process will be provided. Special emphasis will be given to the emerging modality of lifetime-based nanothermometry in light of the new developments in the field.

2. RENP NANOTHERMOMETRY USING PLIR

RENPs normally consist of a low phonon (vibrational) energy host lattice, typically a fluoride, stoichiometrically doped with trivalent rare-earth ions that can act as both sensitizers and activators (Figure 1a).[19] Rare-earth ions have a plethora of 4*f* electronic energy states that lead to innumerable radiative and nonradiative processes after light excitation. In particular, the nonradiative pathways that result from the absorption or emission of lattice phonons are especially temperature-dependent, and thus, the PLIR between the donor and acceptor states will subsequently be influenced by temperature.[14,18] Depending on the different types of doped photoluminescent centers (activators), PLIR nanothermometry is divided into two categories: single center (singly doped) and double center (codoped).[13] A detailed list of different materials used in PLIR, has been previously reported in the literature.[17]

2.1. Single-Center PLIR Nanothermometry

In a single-center nanothermometer, the PLIR is determined by the radiative transitions from two excited energy levels of the same activator to its ground state (as Figure 1b shows). The PLIR parameter, Δ, is presented by[13]

$$\Delta = \frac{I_2}{I_1} = \frac{A_2 h\nu_2 N_{2(T)}}{A_1 h\nu_1 N_{1(T)}} \tag{1}$$

where I_1 and I_2, A_1 and A_2, ν_1 and ν_2 are the photoluminescence intensities, total spontaneous emission rates, and the frequency of transitions from excited states E_1 and E_2 to the ground state E_0 (excited state E_2 is of higher energy than E_1), respectively. h is Planck's constant. $N_{1(T)}$ and $N_{2(T)}$ are the populations of E_1 and E_2 levels, respectively, at a specific temperature T. Since E_1 and E_2 are thermally coupled, the energy difference between them cannot be too large, normally 200−2000 cm^{-1}.[13] This range ensures sufficient thermal energy to enable photons at the lower level to be populated to the upper level and each emission band can be resolved at room temperature. In a thermal equilibrium situation, N_1 and N_2 meet the following rules:

$$\frac{N_2}{N_1} = \frac{g_2}{g_1} \exp\left(-\frac{\delta E}{k_B T}\right) \tag{2}$$

Here, g_1 and g_2 are the degeneracies of the two levels, δE is the energy gap between the barycenters of the two emission bands, and k_B is the Boltzmann constant. Combining eqs 1 and 2, eq 3 is written as

$$\Delta = B \exp\left(-\frac{\delta E}{k_B T}\right) \tag{3}$$

The linear correlation between $\ln(\Delta)$ and $1/T$ can be exploited to obtain a calibration curve for temperature reading. In this equation, the pre-exponential factor $B = A_2 h\nu_2 g_2 / A_1 h\nu_1 g_1$. It is noteworthy that although B is a constant here, it has been shown to be temperature-dependent at sufficiently low temperatures as the reorganization of the populations among Stark sublevels occurs.[22] Practically, the values of δE and B are obtained from a log−log fit from the graph of intensity ratio versus temperature.

To characterize the performance of all types of nanothermometers, the relative sensitivity S_r is defined as

$$S_r = \frac{1}{\Delta}\left|\frac{\partial \Delta}{\partial T}\right| \tag{4}$$

S_r can be expressed in $\%\cdot K^{-1}$ and be used to directly compare the performance of diverse nanothermometers despite different compositions or working mechanisms.[13] Another standard parameter is the temperature uncertainty, δT, which represents

https://doi.org/10.1021/acs.accounts.4c00342
Acc. Chem. Res. 2024, 57, 2653−2664

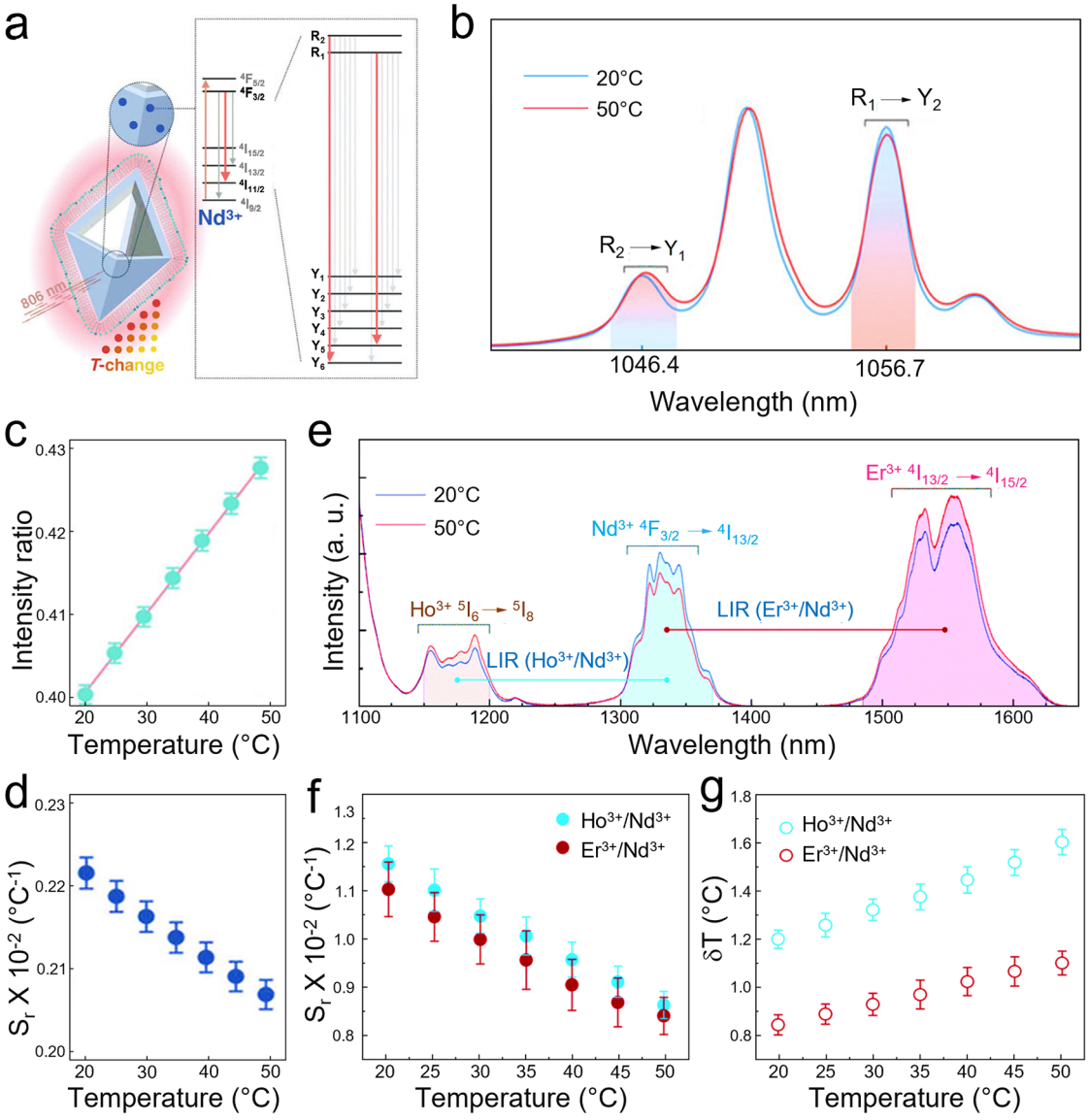

Figure 2. (a) Schematic representation of Nd^{3+}-doped RENP nanothermometry, where the Nd^{3+} energy states (left) and the Stark states of interest (right) are shown. (b) Photoluminescence spectra of Nd^{3+}-doped RENPs at 20 and 50 °C. (c, d) PLIR of $R_2 \rightarrow Y_1$ and $R_1 \rightarrow Y_2$ (c) and the relative sensitivity (d) at varied temperatures. (e) Photoluminescence spectra of Ho^{3+}/Nd^{3+} and Er^{3+}/Nd^{3+} double-center RENPs at 20 and 50 °C. (f, g) Relative thermal sensitivity and the temperature uncertainty for PLIR (Ho^{3+}/Nd^{3+}) and PLIR (Er^{3+}/Nd^{3+}), respectively. Reproduced with permission from ref 2 (Copyright 2019 WILEY-VCH) and ref 28 (Copyright 2017 Royal Society of Chemistry).

the smallest resolved temperature for a given nanothermometer and is estimated as following:[13]

$$\delta T = \frac{1}{S_r}\frac{\delta\Delta}{\Delta} \tag{5}$$

The potential for single-center PLIR nanothermometry has been widely investigated (e.g., Er^{3+}, Eu^{3+}, Nd^{3+}, or Pr^{3+}-doped RENPs).[23−25] Perhaps the most studied are Er^{3+}, Yb^{3+} codoped RENPs.[26] In this classic system, the ion excited in the $^2H_{11/2}$ state of Er^{3+} will nonradiatively decay to the lower-lying $^4S_{3/2}$ state. These two states are in Boltzmann equilibrium and changes in surrounding temperature will cause a rearrangement of their populations (see Figure 1b: single center). The temperature is determined by the PLIR from these thermally coupled states once the calibration curve is obtained. These types of photoluminescent nanothermometers are called secondary nanothermometers since they necessitate an external thermal calibration.[13]

While many original photoluminescent nanothermometers exploited the temperature dependence of upconverted visible emissions, RENPs also show versatile NIR downshifting photoluminescence. In the context of NIR single-center nanothermometers, Nd^{3+} (1060 nm), Ho^{3+} (1150 nm), and Er^{3+} (1550 nm) activators have been reported as promising candidates as secondary NIR nanothermometers.[1,27] However, these activators do not typically possess thermally coupled energy states in the NIR region. Fortunately, the 4*f* states of the rare-earth ions have pronounced Stark splitting in host lattices that exert high crystal field strengths on the dopants. Since some of the Stark sublevels follow the Boltzmann distribution and these transitions can be easily optically resolved, they can be employed in NIR nanothermometry.

https://doi.org/10.1021/acs.accounts.4c00342
Acc. Chem. Res. 2024, 57, 2653−2664

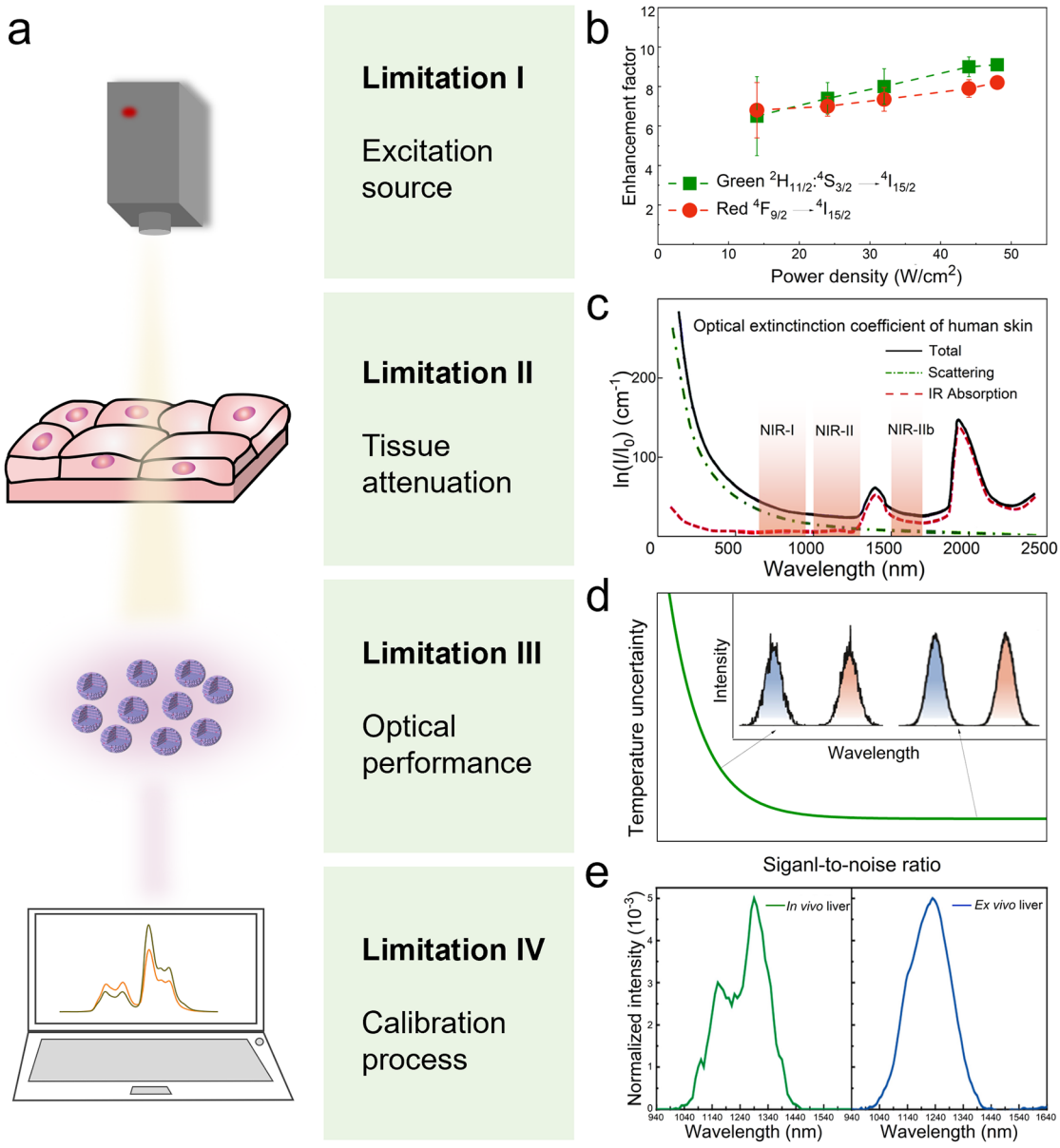

Figure 3. (a) Schematic representation of the complete process of temperature reading in biomedicine. (b) Enhancement factor of upconverted green and red emission bands versus excitation power density. (c) Extinction coefficient of human skin. (d) The temperature reading uncertainty of RENPs with varied signal-to-noise ratios. (e) Emission spectrum *in vivo* and *ex vivo* show the necessity of *in situ* calibration. Adapted with permission from ref 38 (Copyright 2015 WILEY-VCH), ref 39 (Copyright 2014 Materials Research Society), ref 40 (Copyright 2022 American Chemical Society), and ref 41 (Copyright 2020 American Chemical Society).

An example was demonstrated by our group using $LiYF_4:Yb^{3+}$, Tm^{3+}@$LiYF_4$@$LiYF_4:Nd^{3+}$ core−shell RENPs.[2] The Nd^{3+} excited state (in Figure 2a), $^4F_{3/2}$, was further split into thermally coupled R_1 and R_2 Stark states, while the $^4I_{11/2}$ state was split into 6 levels with the Y_1 and Y_2 Stark states participating in the temperature sensing. Specifically, with temperature increase, the intensity of $R_2 \rightarrow Y_1$ (≈1046 nm) increases while $R_1 \rightarrow Y_2$ (≈1056 nm) decreases (Figure 2b, c). The relative thermal sensitivity was ca. 0.22% °C^{-1} at room temperature (Figure 2d), which was the highest among the fluoride-based hosts. The performance of this NIR nanothermometer was successfully evaluated *in vitro* using both 2D and 3D cell cultures and was a major step forward in ultimately demonstrating the feasibility of using Nd^{3+}-doped RENP nanothermometry in a biological setting with an eye on future *in vivo* translational applications.

2.2. Double-Center PLIR Nanothermometry

In the case of double-center nanothermometers, the PLIR is defined by two distinct emission bands from different activators. The temperature dependence of their PLIR is affected by phonon-based processes including nonradiative multiphonon relaxation and nonresonant phonon-assisted energy transfer. Examples of double-center nanothermometers in the visible range have been reported in Eu^{3+}-Tb^{3+}, Pr^{3+}-Tb^{3+}, and Ho^{3+}-Tm^{3+} codoped systems.[29−31] Akin to single-center nanothermometry, attention has lately shifted toward double-center nanothermometers operating in the NIR region.[10,32] An excellent example was demonstrated by Marciniak et al. using

https://doi.org/10.1021/acs.accounts.4c00342
Acc. Chem. Res. 2024, 57, 2653−2664

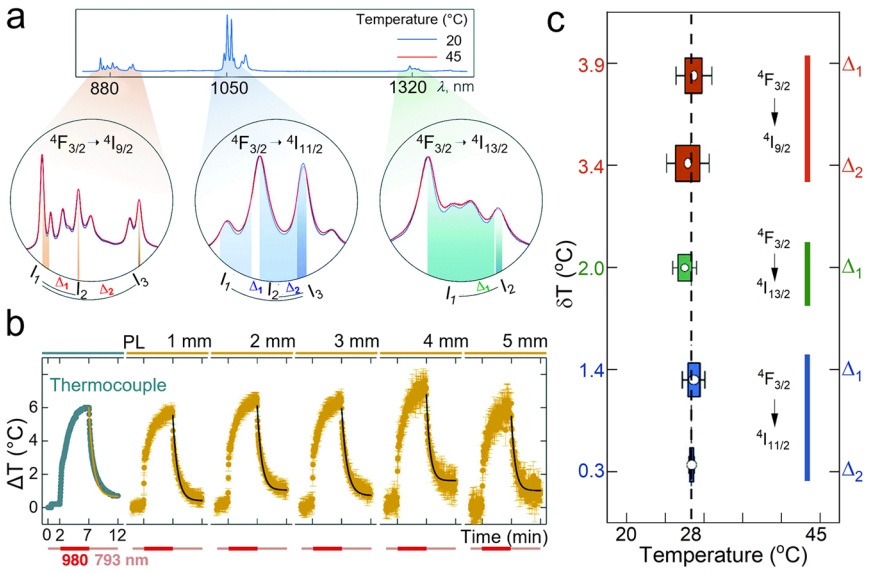

Figure 4. (a) NIR photoluminescence spectra of $LiLuF_4:Nd^{3+}@LiLuF_4$ RENPs at 20 and 45 °C. The individual Nd^{3+} emission bands and their corresponding transitions are spotlighted. (b) Heating−cooling cycles of RENPs measured with a thermocouple (blue-gray color) and NIR nanothermometry (yellow color) through 1−5 mm pork fat. The temperature was obtained following 793 nm excitation using the transition at around 1050 nm as an indicator. (c) Temperature uncertainties of the $LiLuF_4:Nd^{3+}@LiLuF_4$ nanothermometer. Adapted with permission from ref 4. Copyright 2019 Royal Society of Chemistry.

$LiLa_{0.9-x}Nd_{0.1}Yb_xP_4O_{12}$ (x = 0.05−0.5) RENPs.[33] The $Nd^{3+} \rightarrow Yb^{3+}$ energy transfer (ET), a phonon-assisted process, follows the Miyakawa-Dexter model, in which the probability of the interionic energy transfer is expressed as a function of the temperature.[34] Owing to the numerous ET processes, such as phonon-assisted $Nd^{3+} \rightarrow Yb^{3+}$ ET, $Yb^{3+} \rightarrow Nd^{3+}$ back ET, and $Yb^{3+} \rightarrow Yb^{3+}$ energy diffusion, the PLIR between Nd^{3+} ($^4F_{3/2} \rightarrow {}^4I_{9/2}$) and Yb^{3+} ($^2F_{5/2} \rightarrow {}^2F_{7/2}$) emission depend strongly on the temperature as well as concentration of Yb^{3+} ions due to the competition between $Yb^{3+} \rightarrow Nd^{3+}$ and $Yb^{3+} \rightarrow Yb^{3+}$ processes. The best thermometric performance occurs at a Yb^{3+} concentration of 50 mol % with relative sensitivity of 0.4%. In addition, various other NIR double-center nanothermometers that exploit ET mediated by the host/phonons, ions, or ligands have been reported, e.g. Tm^{3+}-Ho^{3+}[30] and Er^{3+}-Ho^{3+}.[27] Our group incorporated Ho^{3+}, Nd^{3+}, and Er^{3+} into $NaGdF_4$ RENPs for double-center PLIR nanothermometry.[28] Due to the phonon-assisted ET in Nd^{3+} ($^4F_{3/2}$) → Yb^{3+} ($^2F_{5/2}$), Yb^{3+} ($^2F_{5/2}$) → Ho^{3+} ($^5I_6$), and Er^{3+} ($^4I_{13/2}$) → Ho^{3+} ($^5I_7$), the PLIR of Ho^{3+}/Nd^{3+}, and Er^{3+}/Nd^{3+} emissions were determined to be temperature dependent (Figure 2e-g). Interestingly, the Ho^{3+} and Er^{3+} temperature-dependent emissions were found to be closely linked to the dispersion solvents, which was ascribed to the O−H assisted nonradiative relaxation. Hence, it must be highlighted that any performance evaluation of nanothermometers intended for biomedical applications must be first and foremost assessed in the aqueous milieu. Otherwise, the same thermally driven optical processes of the nanothermometer dispersed in different solvents cannot be guaranteed and thus the reliability and sensitivity will be affected.

2.3. Limitations of RENP Nanothermometry Using PLIR

Although RENP nanothermometry using PLIR has undergone rapid development and has become a much-studied technique for temperature sensing,[13] recent results point out that the accuracy of PLIR nanothermometry could be put into question. For instance, excitation intensity induced self-heating effects,[35] the variation of photoluminescence intensity at different path lengths through the sample,[36] and the altered sensitivity or disturbed Boltzmann equilibrium at high temperatures[37] can lead to false temperature readout thereby compromising the reliability of the technique. Here, we list possible limitations in PLIR photoluminescence nanothermometry that can originate from the excitation laser, biological tissues, the optical performance of the photoluminescent nanothermometers, and the calibration process (Figure 3a). Finally, we discuss possible strategies to mitigate these problems toward accurate temperature sensing.

2.3.1. Excitation Source. An excitation source has two main characteristics: power density and wavelength. Optimizing the power density of the excitation source is a critical factor. For instance, in the case of $NaGdF_4:Yb^{3+}$, $Er^{3+}@SiO_2$ RENPs, our group showed that the PLIR of $^2H_{11/2}/{}^4S_{3/2} \rightarrow {}^4I_{15/2}$ transition strongly depended on the excitation power density of the 980 nm laser (Figure 3b).[38] Furthermore, Pickel et al. discussed the same phenomenon in detail by modeling the PLIR of the $^2H_{11/2}/{}^4S_{3/2} \rightarrow {}^4I_{15/2}$ transition and showed experimentally that it increased by ∼80% as the excitation power density was increased.[35] To mitigate these artifacts, it is imperative to keep the excitation conditions identical during the temperature measurements and calibration process. Defining a standard excitation power to evaluate the S_r and other performance of each nanothermometer is also strongly recommended.

Continuous laser irradiation would inevitably cause a heating effect, particularly at 980 nm excitation, due to the strong absorption of water molecules. The heating effect does not only affect the accuracy of the temperature readout but may also irreversibly damage the biological samples under study.[42] To avoid errors in temperature sensing caused by heating, minimizing the excitation time by chopping the continuous wave or using a pulsed laser is a feasible option. Another common strategy is to introduce Nd^{3+} as the sensitizer to tune

https://doi.org/10.1021/acs.accounts.4c00342
Acc. Chem. Res. 2024, 57, 2653−2664

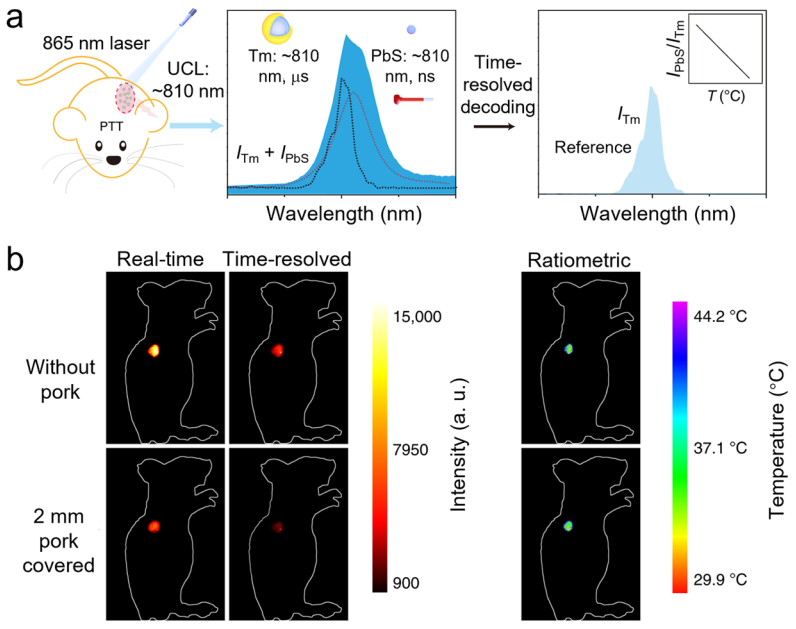

Figure 5. (a) Schematic illustration of the time-resolved PLIR for temperature monitoring *in vivo*. (b) Real-time (I_{total}), time-resolved photoluminescence (I_{Tm}) imaging, and temperature sensing from PLIR nanothermometry with and without a 2 mm pork tissue covering. Reproduced with permission from the ref 50. Copyright 2020 Springer Nature.

the excitation wavelength to a more biocompatible range at about 808 nm, which is considered to be a heating-free wavelength compared with 980 nm.[19] However, it is noteworthy that the safety regulation (European EN60825 and American ANSI Z136.1) allows approximately double the irradiance time for more than 10 s at 980 nm compared with 808 nm (ca. 330 mW cm^{-2}).[43]

2.3.2. Tissue. Another potential source of error could be observed when working with biological tissues. As shown in Figure 3c, the extinction coefficient of tissue, which is mainly attributed to the absorption and scattering effect, is strongly wavelength-dependent. Nanothermometers, particularly RENPs, whose emissions lie in the biological windows (NIR-I: 700−900 nm, NIR-IIa:1300−1400 nm, NIR-IIb:1500−1700 nm) thus offer considerable advantages for accurate temperature reading.[1] Our group synthesized a single-center nanothermometer, $LiLuF_4:Nd^{3+}$@$LiLuF_4$, covering the NIR-I and NIR-IIa windows at around 880 nm ($^4F_{3/2} \rightarrow {}^4I_{9/2}$), 1050 nm ($^4F_{3/2} \rightarrow {}^4I_{11/2}$), and 1320 nm ($^4F_{3/2} \rightarrow {}^4I_{13/2}$), respectively (Figure 4).[4] However, even within the biological window, the acquired δT presented significant deviation changing from 0.19 to 1.23 °C with increased thickness of pork fat tissue from 1 to 5 mm, revealing its validity was highly compromised by tissue thickness.

Tissue components should also be considered in the actual temperature reading. While many different types of biological and phantom tissues have been studied as the *ex vivo* temperature sensing medium, it should be noted that the optical attenuation coefficient and the performance of nanothermometers are noncomparable in different tissues. A particular example was reported using AgS nanothermometer and the same phenomenon also occurred in RENPs.[41] A comprehensive study of the thermally dependent optical properties of tissues could be an approach to solving this problem. Alternatively, employing lifetimes to estimate temperature is another approach to mitigate tissue-induced distortions (*vide infra*).

2.3.3. Optical Performance of Nanothermometers. Low signal-to-noise ratio (SNR) is also a severe problem hindering the further application of RENPs in nanothermometry, as shown in Figure 3d, where the temperature uncertainty of RENPs nanothermometers presents a strongly nonlinear relationship with the SNR ratio.[40] Design and synthesis of RENPs with high quantum yield is thus an urgent but still challenging topic. Many groups have proposed various methods to improve the photoluminescence quantum yield both in upconversion and downshifting (maximum reported 6.34%[44] and 50%,[45] respectively), such as tailoring the local crystal field of the doped activator, surface passivation with core−shell architectures, plasmonic enhancement using noble metals, and utilizing organic fluorophores as ligand antennae.[13,19−21] However, none of these strategies have become mainstream and the community needs to strive toward fostering very bright RENPs. On the other hand, while RENPs have low quantum yields, the actual figure of merit is the SNR, which is comparatively high since they are excited in the NIR region while some of them also emit in the NIR region. Hence, even when the RENP signal is low, the SNR is high as the background autofluorescence is also very low.

In addition to the quantum yield, temperature itself will also affect the photoluminescence intensity of the RENPs. Most of the nanothermometers show decreased intensity under higher temperatures due to the stronger resonance of the host phonon and higher probability of nonradiative relaxation processes. An intriguing positive thermal response also has been observed in $NaYF_4:Yb^{3+}$, Tm^{3+} RENPs.[46] This interesting effect should be further studied such that it can be broadly adopted by the community.

2.3.4. Calibration Process. According to eq 3, knowing the value of δE and B is the key to resolving the temperature in the PLIR method. Based on whether the calibration is necessary to determine the δE and B, the nanothermometers can be classified as primary or secondary types. For secondary nanothermometers, δE and B result from a fit between the

https://doi.org/10.1021/acs.accounts.4c00342
Acc. Chem. Res. 2024, 57, 2653−2664

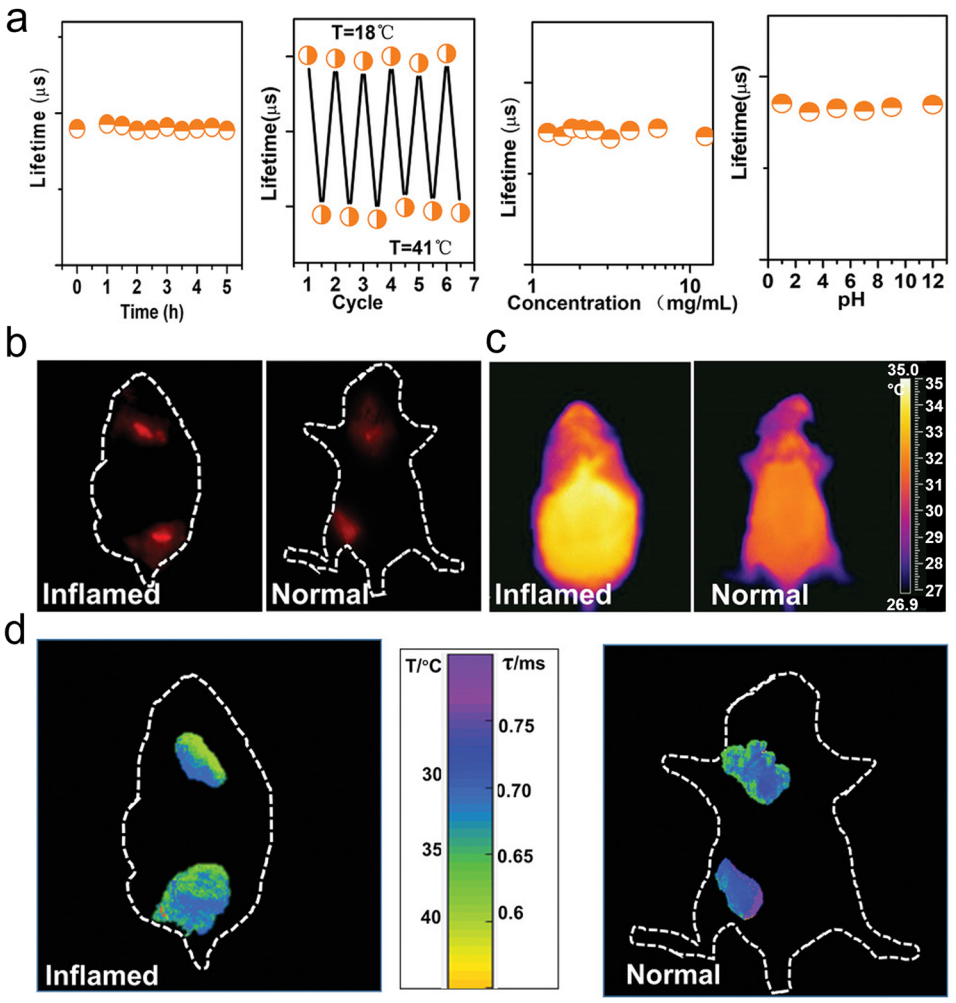

Figure 6. (a) Stability of the photoluminescence lifetime against varied conditions. (b) Thermal images using photoluminescence intensity, (c) thermal camera, and (d) lifetime-based nanothermometry in the inflamed and normal mice, respectively. Reproduced with permission from the ref 12. Copyright 2020 WILEY-VCH.

preset temperature and intensity ratio. Therefore, an additional temperature reference, e.g., thermocouple or thermal camera, is needed for *in situ* thermal calibration (Figure 3e). However, our recent proof-of-concept work demonstrated that thermal cameras can only detect the surface temperature[5] and thus most applications necessitate using physical means of acquiring the reference temperature (e.g., thermocouple), which is especially challenging for *in vivo* studies. More recently, primary nanothermometers have been proposed where δE and B can be determined based on the knowledge of thermodynamic laws and thus do not require calibration.[47,48] A seminal example of a primary nanothermometer was illustrated in SrF_2:Yb^{3+}, Er^{3+} RENPs where δE was calculated using the barycenters of the photoluminescence peaks and B was empirically calculated from the plot of δE versus laser power.[49] This work took a giant stride toward the demonstration that any photoluminescence nanothermometer that can be described using eq 3 has the potential to be a primary nanothermometer. However, it should be noted that to date, no primary nanothermometer in the NIR range has been reported.

3. LIFETIME-BASED RENP NANOTHERMOMETRY

As discussed above, PLIR nanothermometry has been the mainstream method due to the representative thermally coupled states in RENPs. On the other hand, temperature-dependent nonradiative depopulation of the excited states enables photoluminescence lifetime as the contrast mechanism to infer the temperature.

Qiu et al. fabricated a hybrid structure in which emission at around 810 nm could be obtained from both Tm^{3+}-doped RENPs and PbS quantum dots ($I_{total} = I_{Tm} + I_{PbS}$).[50] The overlapped emissions were then decoded via a time-resolved technique due to different photoluminescence lifetimes (Figure 5a). This breakthrough work was the first to show the insensitivity of the nanothermometer to tissue thicknesses due to the same emission band used for PLIR, which minimized the wavelength-induced attenuation coefficient difference of tissue. As Figure 5b demonstrates, although the real-time intensity (I_{total}) or the time-resolved intensity (I_{Tm}) decreased after passing through 2 mm pork tissue, the PLIR ($\frac{I_{total} - I_{Tm}}{I_{Tm}}$) remained unchanged. Time-resolved nanothermometry could be considered as a transition between PLIR and lifetime-based

https://doi.org/10.1021/acs.accounts.4c00342
Acc. Chem. Res. 2024, 57, 2653−2664

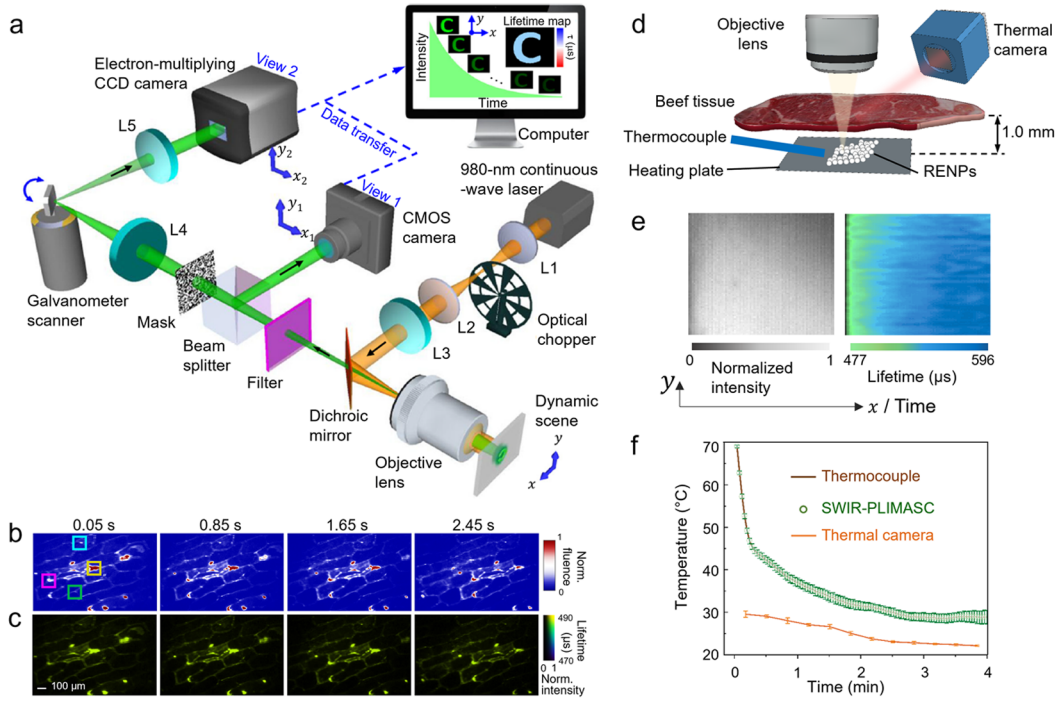

Figure 7. (a) Schematic of the SPLIT system. (b) Time-integrated images of onion epidermis cells labeled with upconverting RENPs. (c) Lifetime images corresponding to (b). (d) Part of the SWIR-PLIMASC system, which also captures single-shot lifetime images of RENPs but operates in the NIR range. (e) Dynamic intensity and temperature mapping while the sample was scanned. (f) Comparison of the temperature readout from SWIR-PLIMASC, thermocouple, and thermal camera. Reproduced with permission from ref 3 (Copyright Springer Nature) and ref 5 (Copyright 2024 WILEY-VCH).

nanothermometry since it introduced a time-resolved method but still essentially relied on the PLIR of two emission peaks.

True photoluminescence lifetime-based nanothermometry is an attractive alternative to the PLIR technique. The photoluminescence lifetime τ of an excited state can be expressed as

$$\tau = \frac{1}{W_r + W_{nr}} \tag{6}$$

Here, W_r and W_{nr} are the radiative and nonradiative decay rates, respectively. W_r is temperature independent since the radiative transition process is mostly determined by the electronic configuration of the ion while W_{nr} is strongly dependent on the existence of multiphonon relaxation, phonon-assisted nonresonant energy transfer, and other nonradiative processes.[12] Therefore, the total lifetime (τ) of the excited state is influenced by temperature and the relationship can be expressed by an Arrhenius-type equation as follows:

$$\frac{1}{\tau} = \frac{1}{\tau_0} + C \exp\left(-\frac{E_A}{K_B T}\right) \tag{7}$$

where $1/\tau_0$ is the temperature-independent decay rate, C is the pre-exponential constant, and E_A is the activation energy.[13]

Notably, the photoluminescence lifetime is an intrinsic property that is less vulnerable to variations due to light penetration depth, the presence of other fluorophores/chromophores (for example in a biological medium), the solvent in which the probe is dispersed, etc.[11,12] It has been confirmed that the photoluminescence lifetime signal maintains a high SNR after an 8 mm penetration depth of intralipid (1%) and was further applied in the biodistribution studies and diagnosis of tumor subtypes.[51,52] Lifetime-based nanothermometry is a robust technique that holds crucial potential to overcome the limitations associated with PLIR nanothermometry.[11,51,53] A typical example in lifetime-based nanothermometry was reported by Tan et al. using $NaYF_4$@$NaYF_4$:Yb^{3+}, Nd^{3+}@CaF_2 RENPs.[12] The lifetime-based nanothermometer was shown to be stable, reliable, and repeatable against different work conditions (in Figure 6a). In contrast to the thermal images using the photoluminescence intensity and thermal camera, photoluminescence lifetime images presented the precise temperature distribution profile in the area with accumulated RENPs. (Figures 6b-d). In Figure 6d, the evaluated average lifetime difference between inflamed and normal mice was 0.2 ms, and the corresponding temperature difference was 2.3 °C, indicating that the obvious lifetime/temperature difference could thus be an effective indicator for inflammation detection.

Despite the aforementioned advantages of photoluminescence lifetime-based nanothermometry, it is still not widely studied due to the high cost and complexity of the instrumentation, low measurement efficiency, and required expertise in data analysis. The most common technology is time-correlated single-photon counting (TCSPC). This technique features single photon detection but is time-consuming in both data acquisition and processing, which impedes the further study of dynamic scenes or two-dimensional views.[54] To accelerate data collection, our group developed single-shot photoluminescence lifetime imaging thermometry (SPLIT).[3] As shown in Figure 7a, this optical system synergistically utilized an encoding mask for spatial information extraction and a galvanometer scanner that temporally shears dynamic scenes for photoluminescence

https://doi.org/10.1021/acs.accounts.4c00342
Acc. Chem. Res. 2024, 57, 2653−2664

lifetime measurement. Largely advancing current lifetime measurement techniques, SPLIT enables two-dimensional video-rate lifetime and temperature mapping of a moving biological sample (Figure 7b, c), bridging the gap between instrument advancement and lifetime-based nanothermometry. To further push the system toward deep tissue temperature sensing, our group subsequently developed SWIR-PLIMASC (Figure 7d) that works in the short-wave infrared (SWIR, or NIR) range. This marks the first of its kind instrument for high sensitivity, high-light throughput, ultrahigh-speed NIR lifetime imaging. SWIR-PLIMASC presents advantages in true temperature sensing while the thermal camera has a large deviation under 0.5 mm-thick beef tissue (Figure 7e, f).[5] We can anticipate the future applications of SWIR-PLIMASC in two-dimensional real-time lifetime mapping and temperature sensing under deep tissue penetration depth.

4. CONCLUSION AND OUTLOOK

In summary, we have discussed the two most commonly used methodologies: PLIR and lifetime-based RENP nanothermometry. Successful applications of RENP nanothermometry have been demonstrated both *in vitro* and *in vivo*. However, it is now largely accepted that in most cases, accurate temperature readout using these RENPs is affected by their surroundings and experimental conditions. The desired nanothermometer will further require high accuracy and reliability for real-time temperature monitoring. Following the discussions above, the performance of RENP nanothermometry can be optimized in three aspects:

First, from the materials perspective, new RENP nanothermometers should be continuously sought to optimize their optical performance such as high photoluminescence intensity, low thermal uncertainty, and tunable lifetime. Further investigation on the possible influential factors of optical performance would aid in eliminating the error sensing of temperature. Second, from a methodology point of view, lifetime-based nanothermometry has great potential for accurate temperature reading and should be studied in more detail. This development should not only concentrate on materials design but also the data collection and processing to realize dynamically temperature sensing with high temporal resolution. Finally, on the instrumentation side, although photoluminescence instrumentation is a mature technology and easily commercially available, only a few reports have used hyperspectral imaging in photoluminescence nanothermometry to demonstrate spatial information together with spectrum details. Hyperspectral imaging, especially operating in the NIR range, would provide more opportunities for accurate PLIR nanothermometry. Meanwhile, with the development of lifetime-based nanothermometry, it is expected that future advancements in instrumentation will prioritize features that are more compact, user-friendly, and tailored for clinic settings, specifically designed in the NIR range.

To become a powerful tool in living systems, research in RENP nanothermometry must adopt an interdisciplinary approach that encompasses materials design, optical engineering, and biological analysis. Thus, future breakthroughs in the development of RENP nanothermometry can only be accomplished through the exchange of ideas and discussions from different fields. Furthermore, RENP nanothermometry will be applied to glean more information about intracellular temperature dynamics, opening a venue for fundamental investigations into the role of thermal fluctuations in living systems, and enabling real-time *in situ* monitoring of the metabolism of diseases *in vivo*.

AUTHOR INFORMATION

Corresponding Authors

Fiorenzo Vetrone − *Centre Énergie Matériaux Télécommunications, Institut National de la Recherche Scientifique, Université du Québec, Varennes, Québec J3X 1P7, Canada;* orcid.org/0000-0002-3222-3052; Email: fiorenzo.vetrone@inrs.ca

Jinyang Liang − *Centre Énergie Matériaux Télécommunications, Institut National de la Recherche Scientifique, Université du Québec, Varennes, Québec J3X 1P7, Canada;* orcid.org/0000-0001-5983-0488; Email: jinyang.liang@inrs.ca

Author

Miao Liu − *Centre Énergie Matériaux Télécommunications, Institut National de la Recherche Scientifique, Université du Québec, Varennes, Québec J3X 1P7, Canada*

Complete contact information is available at: https://pubs.acs.org/10.1021/acs.accounts.4c00342

Author Contributions

M.L.: writing-original draft, writing-review and editing; J.L.: conceptualization (equal), funding acquisition (equal), supervision (equal), writing-original draft (supporting), writing-review and editing (equal); F.V.: conceptualization (equal), funding acquisition (equal), supervision (equal), writing-original draft (lead), writing-review and editing (equal) CRediT: **Miao Liu** conceptualization, data curation, formal analysis, investigation, methodology, software, writing-original draft, writing-review & editing; **Jinyang Liang** conceptualization, formal analysis, funding acquisition, methodology, project administration, resources, supervision, validation, visualization, writing-review & editing; **Fiorenzo Vetrone** conceptualization, data curation, formal analysis, funding acquisition, investigation, methodology, project administration, resources, supervision, validation, visualization, writing-review & editing.

Notes

The authors declare no competing financial interest.

Biographies

Miao Liu is currently a Ph.D. student at Centre Énergie Matériaux Télécommunications, Institut National de la Recherche Scientifique, Université du Québec. Her research interests focus on rare-earth doped nanomaterials, ultrafast imaging microscopy, and nanothermometry in biomedicine.

Jinyang Liang is an Associate Professor at Centre Énergie Matériaux Télécommunications, Institut National de la Recherche Scientifique, Université du Québec. His research interests include the development of new computational imaging systems and their applications in materials characterization, biomedicine, and advanced manufacturing.

Fiorenzo Vetrone is a Full Professor at Centre Énergie Matériaux Télécommunications, Institut National de la Recherche Scientifique, Université du Québec. His research interests focus on the development of rare-earth doped nanoparticles and their implementation in multifunctional nanoplatforms for applications in biological systems and nanomedicine.

https://doi.org/10.1021/acs.accounts.4c00342
Acc. Chem. Res. 2024, 57, 2653−2664

■ ACKNOWLEDGMENTS

The authors thank Dr. Xianglei Liu for fruitful discussion. This work was supported in part by Natural Sciences and Engineering Research Council of Canada (RGPIN-2017-05959, RGPIN-2018-06217, RGPAS-2017-507845, RGPAS-2018-522650, I2IPJ-555593-20); Canada Research Chairs Program (CRC-2022-00119); Canada Foundation for Innovation and Ministère de l'Économie et de l'Innovation du Québec (37146); Canadian Cancer Society (707056); New Frontiers in Research Fund (NFRFE-2020-00267); Fonds de Recherche du Québec–Nature et Technologies (203345–Centre d'Optique, Photonique, et Lasers; 203321-Centre québécois sur les matériaux fonctionnels/Québec Centre for Advanced Materials; 255545-Projet de recherche en équipe); Fonds de Recherche du Québec–Santé (267406, 280229).

■ REFERENCES

(1) Hazra, C.; Skripka, A.; Ribeiro, S. J. L.; Vetrone, F. Erbium Single-Band Nanothermometry in the Third Biological Imaging Window: Potential and Limitations. *Adv. Optical Mater.* **2020**, *8* (23), 2001178–2001186.

(2) Skripka, A.; Karabanovas, V.; Jarockyte, G.; Marin, R.; Tam, V.; Cerruti, M.; Rotomskis, R.; Vetrone, F. Decoupling Theranostics with Rare Earth Doped Nanoparticles. *Adv. Funct. Mater.* **2019**, *29* (12), 1807105–1807116.

(3) Liu, X.; Skripka, A.; Lai, Y.; Jiang, C.; Liu, J.; Vetrone, F.; Liang, J. Fast Wide-Field Upconversion Luminescence Lifetime Thermometry Enabled by Single-Shot Compressed Ultrahigh-Speed Imaging. *Nat. Commun.* **2021**, *12* (1), 6401–6409.

(4) Skripka, A.; Morinvil, A.; Matulionyte, M.; Cheng, T.; Vetrone, F. Advancing Neodymium Single-Band Nanothermometry. *Nanoscale* **2019**, *11* (23), 11322–11330.

(5) Liu, M.; Lai, Y.; Marquez, M.; Vetrone, F.; Liang, J. Short-Wave Infrared Photoluminescence Lifetime Mapping of Rare-Earth Doped Nanoparticles Using All-optical Streak Imaging. *Adv. Sci.* **2024**, *11* (11), 2305284–2305292.

(6) Evans, S. S.; Repasky, E. A.; Fisher, D. T. Fever and the Thermal Regulation of Immunity: the Immune System Feels the Heat. *Nat. Rev. Immunol.* **2015**, *15* (6), 335–349.

(7) Daniel, R. M.; Danson, M. J.; Eisenthal, R.; Lee, C. K.; Peterson, M. E. The Effect of Temperature on Enzyme Activity: New Insights and Their Implications. *Extremophiles* **2008**, *12* (1), 51–59.

(8) Campbell-Staton, S. C.; Velotta, J. P.; Winchell, K. M. Selection on Adaptive and Maladaptive Gene Expression Plasticity During Thermal Adaptation to Urban Heat Islands. *Nat. Commun.* **2021**, *12* (1), 6195–6208.

(9) Rodriguez-Sevilla, P.; Marin, R.; Ximendes, E.; Del Rosal, B.; Benayas, A.; Jaque, D. Luminescence Thermometry for Brain Activity Monitoring: A Perspective. *Front. Chem.* **2022**, *10*, 941861.

(10) Ximendes, E. C.; Santos, W. Q.; Rocha, U.; Kagola, U. K.; Sanz-Rodriguez, F.; Fernandez, N.; Gouveia-Neto, A. d. S.; Bravo, D.; Domingo, A. M.; del Rosal, B.; et al. Unveiling In Vivo Subcutaneous Thermal Dynamics by Infrared Luminescent Nanothermometers. *Nano Lett.* **2016**, *16* (3), 1695–1703.

(11) Shen, Y.; Lifante, J.; Zabala-Gutierrez, I.; de la Fuente-Fernandez, M.; Granado, M.; Fernandez, N.; Rubio-Retama, J.; Jaque, D.; Marin, R.; Ximendes, E.; Benayas, A. Reliable and Remote Monitoring of Absolute Temperature during Liver Inflammation via Luminescence-Lifetime-Based Nanothermometry. *Adv. Mater.* **2022**, *34* (7), 2107764–2107773.

(12) Tan, M.; Li, F.; Cao, N.; Li, H.; Wang, X.; Zhang, C.; Jaque, D.; Chen, G. Accurate In Vivo Nanothermometry Through NIR-II Lanthanide Luminescence Lifetime. *Small* **2020**, *16* (48), 2004118–2004127.

(13) Brites, C. D. S.; Balabhadra, S.; Carlos, L. D. Lanthanide-Based Thermometers: At the Cutting-Edge of Luminescence Thermometry. *Adv. Optical Mater.* **2019**, *7* (5), 1801239–1801268.

(14) Wang, X. D.; Wolfbeis, O. S.; Meier, R. J. Luminescent Probes and Sensors for Temperature. *Chem. Soc. Rev.* **2013**, *42* (19), 7834–7869.

(15) Jaque, D.; Vetrone, F. Luminescence Nanothermometry. *Nanoscale* **2012**, *4* (15), 4301–4326.

(16) Zhou, J.; Del Rosal, B.; Jaque, D.; Uchiyama, S.; Jin, D. Advances and Challenges for Fluorescence Nanothermometry. *Nat. Methods* **2020**, *17* (10), 967–980.

(17) Wolfbeis, O. S. An Overview of Nanoparticles Commonly Used in Fluorescent Bioimaging. *Chem. Soc. Rev.* **2015**, *44* (14), 4743–4768.

(18) Gai, S.; Li, C.; Yang, P.; Lin, J. Recent Progress in Rare Earth Micro/Nanocrystals: Soft Chemical Synthesis, Luminescent Properties, and Biomedical Applications. *Chem. Rev.* **2014**, *114* (4), 2343–2389.

(19) Matulionyte, M.; Skripka, A.; Ramos-Guerra, A.; Benayas, A.; Vetrone, F. The Coming of Age of Neodymium: Redefining Its Role in Rare Earth Doped Nanoparticles. *Chem. Rev.* **2023**, *123* (1), 515–554.

(20) Dong, H.; Du, S. R.; Zheng, X. Y.; Lyu, G. M.; Sun, L. D.; Li, L. D.; Zhang, P. Z.; Zhang, C.; Yan, C. H. Lanthanide Nanoparticles: From Design toward Bioimaging and Therapy. *Chem. Rev.* **2015**, *115* (19), 10725–10815.

(21) Bednarkiewicz, A.; Marciniak, L.; Carlos, L. D.; Jaque, D. Standardizing Luminescence Nanothermometry for Biomedical Applications. *Nanoscale* **2020**, *12* (27), 14405–14421.

(22) Suta, M.; Meijerink, A. A Theoretical Framework for Ratiometric Single Ion Luminescent Thermometers—Thermodynamic and Kinetic Guidelines for Optimized Performance. *Adv. Theory Simul.* **2020**, *3* (12), 2000176–2000207.

(23) Lucchini, G.; Speghini, A.; Canton, P.; Vetrone, F.; Quintanilla, M. Engineering Efficient Upconverting Nanothermometers using Eu^{3+} ions. *Nanoscale Adv.* **2019**, *1* (2), 757–764.

(24) Brites, C. D. S.; Fiaczyk, K.; Ramalho, J. F. C. B.; Sójka, M.; Carlos, L. D.; Zych, E. Widening the Temperature Range of Luminescent Thermometers Through the Intra-and Interconfigurational Transitions of Pr^{3+}. *Adv. Optical Mater.* **2018**, *6* (10), 1701318–1701322.

(25) Cantarano, A.; Yao, J.; Matulionyte, M.; Lifante, J.; Benayas, A.; Ortgies, D. H.; Vetrone, F.; Ibanez, A.; Gerardin, C.; Jaque, D.; Dantelle, G. Autofluorescence-Free In Vivo Imaging Using Polymer-Stabilized Nd^{3+}-Doped YAG Nanocrystals. *ACS Appl. Mater. Interfaces* **2020**, *12* (46), 51273–51284.

(26) Vetrone, F.; Naccache, R.; Zamarrón, A.; Juarranz de la Fuente, A.; Sanz-Rodríguez, F.; Martinez Maestro, L.; Martín Rodriguez, E.; Jaque, D.; García Solé, J.; Capobianco, J. A. Temperature Sensing Using Fluorescent Nanothermometers. *ACS Nano* **2010**, *4* (6), 3254–3258.

(27) Jia, M.; Fu, Z.; Liu, G.; Sun, Z.; Li, P.; Zhang, A.; Lin, F.; Hou, B.; Chen, G. NIR-II/III Luminescence Ratiometric Nanothermometry with Phonon-Tuned Sensitivity. *Adv. Optical Mater.* **2020**, *8* (6), 1901173–1901179.

(28) Skripka, A.; Benayas, A.; Marin, R.; Canton, P.; Hemmer, E.; Vetrone, F. Double Rare-Earth Nanothermometer in Aqueous Media: Opening the Third Optical Transparency Window to Temperature Sensing. *Nanoscale* **2017**, *9* (9), 3079–3085.

(29) Gao, Y.; Huang, F.; Lin, H.; Zhou, J.; Xu, J.; Wang, Y. A Novel Optical Thermometry Strategy Based on Diverse Thermal Response from Two Intervalence Charge Transfer States. *Adv. Funct. Mater.* **2016**, *26* (18), 3139–3145.

(30) Savchuk, O. A.; Carvajal, J. J.; Brites, C. D. S.; Carlos, L. D.; Aguilo, M.; Diaz, F. Upconversion Thermometry: A New Tool to Measure the Thermal Resistance of Nanoparticles. *Nanoscale* **2018**, *10* (14), 6602–6610.

(31) Brites, C. D.; Lima, P. P.; Silva, N. J.; Millan, A.; Amaral, V. S.; Palacio, F.; Carlos, L. D. A Luminescent Molecular Thermometer for Long-Term Absolute Temperature Measurements at the Nanoscale. *Adv. Mater.* **2010**, *22* (40), 4499–4504.

https://doi.org/10.1021/acs.accounts.4c00342
Acc. Chem. Res. 2024, 57, 2653–2664

(32) Carrasco, E.; del Rosal, B.; Sanz-Rodríguez, F.; de la Fuente, Á. J.; Gonzalez, P. H.; Rocha, U.; Kumar, K. U.; Jacinto, C.; Solé, J. G.; Jaque, D. Intratumoral Thermal Reading During Photo-Thermal Therapy by Multifunctional Fluorescent Nanoparticles. *Adv. Funct. Mater.* **2015**, *25* (4), 615−626.
(33) Marciniak, L.; Bednarkiewicz, A.; Stefanski, M.; Tomala, R.; Hreniak, D.; Strek, W. Near Infrared Absorbing Near Infrared Emitting Highly-Sensitive Luminescent Nanothermometer Based on Nd^{3+} to Yb^{3+} Energy Transfer. *Phys. Chem. Chem. Phys.* **2015**, *17* (37), 24315−24321.
(34) Miyakawa, T.; Dexter, D. L. Phonon Sidebands, Multiphonon Relaxation of Excited States, and Phonon-Assisted Energy Transfer between Ions in Solids. *Phys. Rev. B* **1970**, *1* (7), 2961−2969.
(35) Pickel, A. D.; Teitelboim, A.; Chan, E. M.; Borys, N. J.; Schuck, P. J.; Dames, C. Apparent Self-Heating of Individual Upconverting Nanoparticle Thermometers. *Nat. Commun.* **2018**, *9* (1), 4907−4918.
(36) Pérez-Rodríguez, C.; Martín, L. L.; León-Luis, S. F.; Martín, I. R.; Kumar, K. K.; Jayasankar, C. K. Relevance of Radiative Transfer Processes on Nd^{3+} Doped Phosphate Glasses for Temperature Sensing by Means of the Fluorescence Intensity Ratio Technique. *Sens. Actuators, B* **2014**, *195*, 324−331.
(37) Geitenbeek, R. G.; de Wijn, H. W.; Meijerink, A. Non-Boltzmann Luminescence in $NaYF_4$:Eu^{3+}: Implications for Luminescence Thermometry. *Phys. Rev. Applied* **2018**, *10* (6), 064006−064015.
(38) Rohani, S.; Quintanilla, M.; Tuccio, S.; De Angelis, F.; Cantelar, E.; Govorov, A. O.; Razzari, L.; Vetrone, F. Enhanced Luminescence, Collective Heating, and Nanothermometry in an Ensemble System Composed of Lanthanide-Doped Upconverting Nanoparticles and Gold Nanorods. *Adv. Optical Mater.* **2015**, *3* (11), 1606−1613.
(39) Hemmer, E.; Vetrone, F.; Soga, K. Lanthanide-Based Nanostructures for Optical Bioimaging: Small Particles with Large Promise. *MRS Bull.* **2014**, *39* (11), 960−964.
(40) van Swieten, T. P.; Meijerink, A.; Rabouw, F. T. Impact of Noise and Background on Measurement Uncertainties in Luminescence Thermometry. *ACS Photonics* **2022**, *9* (4), 1366−1374.
(41) Shen, Y.; Lifante, J.; Fernandez, N.; Jaque, D.; Ximendes, E. In Vivo Spectral Distortions of Infrared Luminescent Nanothermometers Compromise Their Reliability. *ACS Nano* **2020**, *14* (4), 4122−4133.
(42) Xie, X.; Liu, X. Photonics: Upconversion Goes Broadband. *Nat. Mater.* **2012**, *11* (10), 842−843.
(43) Nsubuga, A.; Morice, K.; Fayad, N.; Pini, F.; Josserand, V.; Le Guével, X.; Alhabi, A.; Henry, M.; Puchán Sánchez, D.; Plassais, N. et al. Sub 20 nm Upconversion Photosensitizers for Near-Infrared Photodynamic Theranostics. *Adv. Funct. Mater.* **2024**, 2410077 DOI: 10.1002/adfm.202410077.
(44) Zhou, B.; Tang, B.; Zhang, C.; Qin, C.; Gu, Z.; Ma, Y.; Zhai, T.; Yao, J. Enhancing Multiphoton Upconversion Through Interfacial Energy Transfer in Multilayered Nanoparticles. *Nat. Commun.* **2020**, *11* (1), 1174.
(45) Arteaga Cardona, F.; Jain, N.; Popescu, R.; Busko, D.; Madirov, E.; Arus, B. A.; Gerthsen, D.; De Backer, A.; Bals, S.; Bruns, O. T.; et al. Preventing Cation Intermixing Enables 50% Quantum Yield in Sub-15 nm Short-Wave Infrared-Emitting Rare-Earth based Core-shell Nanocrystals. *Nat. Commun.* **2023**, *14* (1), 4462.
(46) Zhou, J.; Wen, S.; Liao, J.; Clarke, C.; Tawfik, S. A.; Ren, W.; Mi, C.; Wang, F.; Jin, D. Activation of the Surface Dark-Layer to Enhance Upconversion in A Thermal Field. *Nat. Photonics* **2018**, *12* (3), 154−158.
(47) Martínez, E. D.; Brites, C. D. S.; Carlos, L. D.; García-Flores, A. F.; Urbano, R. R.; Rettori, C. Electrochromic Switch Devices Mixing Small- and Large-Sized Upconverting Nanocrystals. *Adv. Funct. Mater.* **2019**, *29* (8), 1807758−1807769.
(48) Judd, B. R. Optical Absorption Intensities of Rare-Earth Ions. *Phys. Rev.* **1962**, *127* (3), 750−761.
(49) Balabhadra, S.; Debasu, M. L.; Brites, C. D. S.; Ferreira, R. A. S.; Carlos, L. D. Upconverting Nanoparticles Working As Primary Thermometers In Different Media. *J. Phys. Chem. C* **2017**, *121* (25), 13962−13968.
(50) Qiu, X.; Zhou, Q.; Zhu, X.; Wu, Z.; Feng, W.; Li, F. Ratiometric Upconversion Nanothermometry with Dual Emission at the Same Wavelength Decoded via a Time-Resolved Technique. *Nat. Commun.* **2020**, *11* (1), 4.
(51) Fan, Y.; Wang, P.; Lu, Y.; Wang, R.; Zhou, L.; Zheng, X.; Li, X.; Piper, J. A.; Zhang, F. Lifetime-Engineered NIR-II Nanoparticles Unlock Multiplexed In Vivo Imaging. *Nat. Nanotechnol.* **2018**, *13* (10), 941−946.
(52) Ortgies, D. H.; Tan, M.; Ximendes, E. C.; Del Rosal, B.; Hu, J.; Xu, L.; Wang, X.; Martin Rodriguez, E.; Jacinto, C.; Fernandez, N.; et al. Lifetime-Encoded Infrared-Emitting Nanoparticles for in Vivo Multiplexed Imaging. *ACS Nano* **2018**, *12* (5), 4362−4368.
(53) Okabe, K.; Inada, N.; Gota, C.; Harada, Y.; Funatsu, T.; Uchiyama, S. Intracellular Temperature Mapping with a Fluorescent Polymeric Thermometer and Fluorescence Lifetime Imaging Microscopy. *Nat. Commun.* **2012**, *3*, 705−713.
(54) Sen, R.; Hirvonen, L. M.; Zhdanov, A.; Svihra, P.; Andersson-Engels, S.; Nomerotski, A.; Papkovsky, D. New Luminescence Lifetime Macro-Imager Based on A Tpx3Cam Optical Camera. *Biomed. Opt. Express* **2020**, *11* (1), 77−88.

https://doi.org/10.1021/acs.accounts.4c00342
Acc. Chem. Res. 2024, 57, 2653−2664